RSC Applied Polymers

ROYAL SOCIETY OF CHEMISTRY

PAPER

View Article Online
View Journal | View Issue

Cite this: *RSC Appl. Polym.*, 2024, **2**, 870

Iodonium functionalized polystyrene as non-chemically amplified resists for electron beam and extreme ultraviolet lithography†

Xindi Yao,[a] Peng Lian,[a] Jinping Chen, *[a] Yi Zeng, [a] Tianjun Yu, [a] Shuangqing Wang, [b] Xudong Guo,[b] Rui Hu, [b] Peng Tian,[c] Michaela Vockenhuber,[c] Dimitrios Kazazis, [c] Yasin Ekinci,*[c] Guoqiang Yang *[b] and Yi Li *[a]

A novel non-chemically amplified resist (n-CAR) based on biphenyl iodonium perfluoro-1-butanesulfonate-modified polystyrene with a naphthalimide scaffold ($PSNA_{0.4}$) was synthesized and characterized. Through extensive exploration using dose-dependent resist thickness analysis, acetonitrile was identified as the optimal developer. Employing electron beam lithography (EBL), the n-CAR of $PSNA_{0.4}$ demonstrated its high-resolution patterning capability by resolving a dense line pattern of 18 nm L/S at an exposure dose of 1300 μC cm^{-2}, achieving a high contrast of 7.1. Further studies using extreme ultraviolet lithography (EUVL) demonstrated that the $PSNA_{0.4}$ resist can achieve 22 nm L/S patterns at a dose of 90.8 mJ cm^{-2}, underscoring its high sensitivity for n-CARs. Detailed studies to gain insights into the underlying patterning mechanisms using X-ray photoelectron spectroscopy (XPS) suggest that the cleavage of polar iodonium into nonpolar polystyrene (PS)-based iodobenzene species enables a solubility switch, resulting in negative lithographic patterns. These findings highlight the innovative potential of the $PSNA_{0.4}$ resist in advancing the capabilities of n-CAR technologies, particularly in the realms of EBL and EUVL, for high-resolution lithographic applications.

Received 20th April 2024,
Accepted 16th June 2024

DOI: 10.1039/d4lp00136b

rsc.li/rscapplpolym

Introduction

Recent years have witnessed the ever-growing need for shrinking feature sizes and performance improvements of integrated circuits (ICs) which follow Moore's law.[1] Central to IC fabrication is lithography, the pivotal process defining device feature sizes. Within this landscape, electron beam lithography (EBL) and extreme ultraviolet lithography (EUVL) stand out as frontrunners, where EBL is employed for mask writing and academic research and EUVL is essential for sub-7 nm node IC manufacturing.[2] Consequently, the innovation of new resist materials that meet the stringent demands of EBL and EUVL remains a critical frontier in nanolithography.

For decades, chemically amplified resists (CARs) have dominated the resist market due to their high sensitivity.[3] A typical CAR composition contains a blend of resin, photo-acid generator (PAG), quenchers, and various trace additives. Upon exposure, the released acid will catalytically remove acid labile groups on the side chain of resin, which triggers the solubility change of resin in developers.[4,5] The intrinsic "mixed" nature of CARs leads to the stochastic distribution of PAGs and quenchers. Moreover, inherent acid diffusion is another stochastic issue.[6–8] These factors induce great difficulty in simultaneously optimizing resolution (*R*), line edge roughness (LER), and sensitivity (*S*), which limits CARs to obtain high resolution patterns with good quality.[9] Innovations have been explored, such as integrating PAGs into polymers *via* covalent bonds[10–12] or introducing quenchers to mitigate acid diffusion,[13–16] yet minimizing acid diffusion at diminishing feature sizes is challenging and always comes with a decrease in sensitivity.

To address the issues, considerable attention has been paid to non-chemically amplified resists (n-CARs) in recent years.[17] Typically, n-CARs can be designed as a kind of "one

[a]*Key Laboratory of Photochemical Conversion and Optoelectronic Materials, Technical Institute of Physics and Chemistry, University of Chinese Academy of Sciences, Chinese Academy of Sciences, Beijing 100190, China. E-mail: chenjp@mail.ipc.ac.cn, yili@mail.ipc.ac.cn*
[b]*Key Laboratory of Photochemistry, Institute of Chemistry, University of Chinese Academy of Sciences, Chinese Academy of Sciences, Beijing 100190, China. E-mail: gqyang@iccas.ac.cn*
[c]*Laboratory for X-ray Nanoscience and Technologies, Paul Scherrer Institute, Villigen CH-5232, Switzerland. E-mail: yasin.ekinci@psi.ch*

†Electronic supplementary information (ESI) available: Characterization of $PSNA_{0.4}$ and the films; solubility characterization and lithographic performances of the resist in different organic developers; normalized remaining thickness (NRT) analysis; LER measurement of high-resolution SEM images; mechanistic analysis of $PSNA_{0.4}$ resist pattern generations; etch resistance and pattern transfer capability of the $PSNA_{0.4}$ resist. See DOI: https://doi.org/10.1039/d4lp00136b

component" resist where photosensitive groups are integrated into the polymer backbone and are called "chain scission resists"[18,19] or "self-immolative resists".[20,21] Numerous chain scission type n-CARs such as PMMA,[22] poly(olefin sulfones),[23] and polycarbonate,[24,25] have been developed. Although their resolution is in the range of 20–30 nm, their sensitivity is significantly lower than that of the CARs.[26–29] The exposure doses for most of the non-CARs are over 100 mJ cm^{-1}, while they are generally under 40 mJ $cm^{-1}$for CARs.

One way to improve the sensitivity of n-CARs is to increase the absorption cross-section of the resist material for EUV photons or electron beams. Metal moieties have been introduced into resist materials due to their large absorption cross-sections for EUV. Various kinds of metal based n-CARs, *e.g.* metal-oxo clusters,[30–33] metal oxide nanoparticle resists,[34–37] molecular organometallic resists,[38–40] and polymer-based organometallic resists,[41] have been reported. Cardineau *et al.*[30] reported the synthesis and EUV lithographic evaluation of tin-oxo clusters $[(RSn)_{12}O_{14}(OH)_6]X_2$, and the spherical tin-oxo cage resist printed 18 nm lines at a relatively high dose of 350 mJ cm^{-2}. Recently, Peng *et al.* reported a resist based on a kind of zinc-oxo cluster (Zn-VBA) with an accurate size of 2.2 nm, which resolved a 100 nm pitch pattern at a dose of 92.5 mJ cm^{-2}.[42] Another method to increase the sensitivity is to improve the reaction efficiency of photosensitive groups. In this case, the photosensitive groups serve as pendants on the side chains. The degradation of the sensitive groups upon exposure results in a solubility switch, which avoids the stochastic issues and acid diffusion brought about by the complicated components of CARs.[43]

Gonsalves *et al.* developed a series of sulfonium based polymeric resists and most of them were capable of resolving 20 nm line patterns.[44–47] Among them, the hybrid polymeric resist MAPDST-TIPMA,[47] integrating an organo-iodine part into the polymer structure, achieved 16 nm L/S features at 600 μC cm^{-2} by e-beam irradiation and showed excellent sensitivity at ~6 μC cm^{-2} by a helium ion beam. Our research group has reported a few kinds of sulfonium based n-CARs,[48–50] which realized patterning performance down to 13 nm L/S at exposure doses of 180–200 mJ cm^{-2}. These results suggest that the photosensitive groups have a significant effect on the sensitivity of the resists.

Biphenyl iodonium groups have been reported as PAGs with high photoacid generation efficiency.[51,52] Compared with sulfonium groups, iodonium enjoys a larger absorption cross-section in EUV sources, hence contributing to superior performance in sensitivity.[53] Furthermore, iodonium exhibits a higher decomposition efficiency than sulfonium by ultraviolet irradiation.[54] Although iodonium salts are widely used as PAGs in CAR formulas, they have rarely been applied to n-CARs to achieve better sensitivity while maintaining good resolution. Here, we report a novel n-CAR based on biphenyl iodonium perfluoro-1-butanesufonate-modified polystyrene ($PSNA_{0.4}$). The incorporation of the bulky 1,8-naphthalimide group into the polymer is aimed at improving the film-forming capabilities and the solubility of the resist, as well as facilitating a solubility switch before and after exposure. Furthermore, the introduction of the 1,8-naphthalimide group serves to lower the bond association energy of the phenyl–I bond,[55] thereby increasing the potential sensitivity to exposure. The "one-component" $PSNA_{0.4}$ resist was extensively evaluated by EBL and EUVL, achieving HPs of 18 and 22 nm line/space patterns at doses of 1300 μC cm^{-2} and 90.8 mJ cm^{-2}, respectively. The exposure mechanism of the $PSNA_{0.4}$ resist was investigated using X-ray photoelectron spectroscopy (XPS), revealing an exposure mechanism where the decomposition of polar biphenyl iodonium into radical species $PS^{\bullet}$ and $Naph\text{-}Ar\text{-}I^{+\bullet}$ further leads to nonpolar polystyrene (PS)-based iodobenzene species.

Results and discussion

Synthesis and characterization of $PSNA_{0.4}$

The synthesis procedure for $PSNA_{0.4}$ is depicted in Scheme 1. The polystyrene (PS) precursor was prepared using the method we previously reported[48] with a small molecular weight (M_w = 4.7 × 10^3) and a narrow polydispersity index (PDI = 1.08) (Fig. S1 and S2†). Treatment of PS with *N*-(*p*-iodophenyl)-1,8-naphthalimide (NA) in the presence of *m*-chloroperoxybenzoic acid (*m*-CPBA) and perfluoro-1-butanesulfonic acid in dichloro-

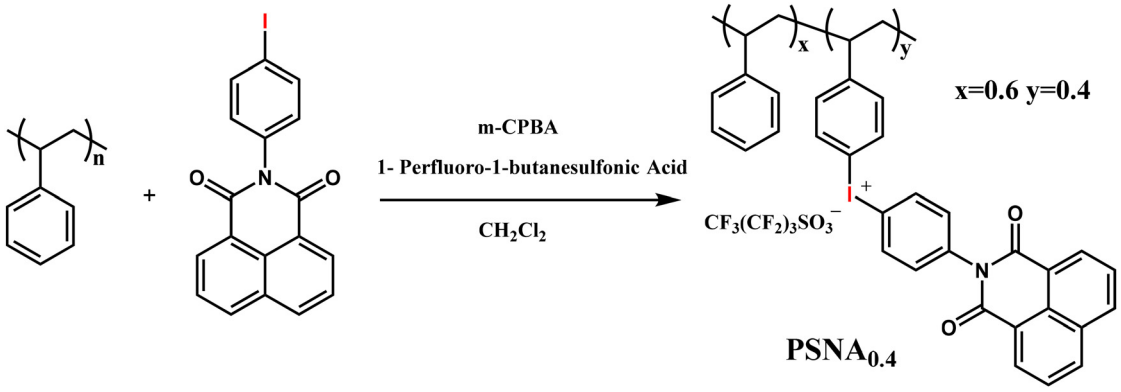

Scheme 1 The synthetic route of $PSNA_{0.4}$.

methane provided $PSNA_{0.4}$ in high yield (65%). It should be noted that the loading ratio of NA is limited to less than 0.5 even if the molar ratio of NA is increased, which may be due to the steric bulk of NA and the resulting product's insolubility. The iodonium content of PS can be adjusted within a low range by varying the feeding ratios of NA. In this study, $PSNA_{0.4}$ is used as the resist material considering the good repeatability of preparation and a relatively high loading ratio where possible. Our previous study demonstrated that a higher loading ratio of sensitive groups contributes to the formation of high-resolution patterns.[49]

The synthesized $PSNA_{0.4}$ was characterized by ^1H NMR spectra (Fig. S4†). Signal peaks located at 6.59–8.50 ppm were attributed to the aromatic protons of benzene and naphthalene rings, and peaks at 1.20–1.90 ppm were assigned to the alkyl protons on the polymer chain of PS. The theoretical ratio of the alkyl protons to the aromatic protons in unmodified and fully modified polystyrene is 3 : 5 and 3 : 14, respectively. $PSNA_{0.4}$ shows a ratio of 3 : 8.5 for the alkyl protons to the aromatic protons, allowing the determination of the loading ratio of iodonium to be 40%. Based on the molecular weight of the PS precursor, the molecular weight of $PSNA_{0.4}$ was calculated to be 17 000 Da. The successful incorporation of the iodonium NA group was further demonstrated by comparing the FTIR spectra of PS and $PSNA_{0.4}$ (Fig. S5†). The absorption band at 1673 cm^{-1} was assigned to the stretching vibration of C=O in the amide group. The peaks located from 1120 to 1350 cm^{-1} were ascribed to the stretching vibration of CF_3 or CF_2 bonds, and the bands at 1133, 1054, and 659 cm^{-1} were attributed to SO_2 symmetric stretching, S–O stretching, and SO_2 deformation, respectively. The new band at 527 cm^{-1} originated from C–I stretching, suggesting the formation of the iodonium structure.

Physical properties of $PSNA_{0.4}$

To meet the requirements of resist materials, physical properties such as solubility, film forming ability, and thermal stability have to be evaluated. $PSNA_{0.4}$ shows good solubility in organic solvents with strong polarity, such as dimethylformamide (DMF), dimethyl sulfoxide (DMSO), acetonitrile, and *n*-butyl lactate (*n*-BL), which reaches more than 100 mg ml^{-1} in each solvent. The thermal behavior of $PSNA_{0.4}$ was investigated by thermogravimetric analysis (TGA) and differential scanning calorimetry (DSC). The TGA curve of $PSNA_{0.4}$ shows a one-stage decomposition process at about 248 °C (Fig. S6a†), indicating good thermal resistance in lithographic evaluation. A glass transition temperature (T_g) of 154 °C was observed by DSC measurement (Fig. S6b†), revealing a relatively rigid structure of $PSNA_{0.4}$. Both the TGA and DSC results confirm that $PSNA_{0.4}$ can endure the baking process in lithography. The surface topography of the spin-coated $PSNA_{0.4}$ film on the wafer was examined by atomic force microscopy (AFM). The root mean square (RMS) roughness of the $PSNA_{0.4}$ film surface is merely 0.30 nm in an area of 10 × 10 μm^2 as measured in 2D AFM pictures (Fig. S7†). These results confirm the potential of $PSNA_{0.4}$ as a promising candidate as a resist material in high resolution lithography.

Optimization of the developing conditions

The introduction of iodonium into the side chain of PS reduces the solubility of $PSNA_{0.4}$ in less polar organic solvents, while it greatly enhances the solubility in polar solvents such as acetonitrile and DMSO. Various kinds of solvents were tested to obtain the sharpest solubility switch of the resist film. The solubility characteristics of $PSNA_{0.4}$ resist films after over-exposure to UV (254 nm) light were examined together with the unexposed film in different developers. The thicknesses of the thin film after baking and after development (with and without exposure) were measured using a spectroscopic ellipsometer. The results are summarized in Table S1.† Less polar solvents such as cyclohexyl chloride, toluene, *n*-butyl acetate, 1,4-dioxane, and MIBK failed to remove the exposed film, not providing a sufficient solubility switch for positive tone development (PTD). While in the case of high polar solvents such as DMSO and isopropyl alcohol (IPA), the exposed and unexposed films are both removed thoroughly or both left unremoved completely. Acetonitrile and *n*-butyl lactate (*n*-BL) are identified as potential developers for NTD due to their excellent selectivity for exposed and unexposed films. Fig. S8† shows the micrometer size patterns of the $PSNA_{0.4}$ resist by 254 nm lithography developed in acetonitrile and *n*-BL, which preliminarily indicate their ability as developers in NTD for the $PSNA_{0.4}$ resist. To optimize the developing conditions, ratios of acetonitrile and *n*-BL in the developer were further studied in the EBL experiment to obtain the best resolution and sensitivity. Fig. S9† shows the 25, 30, and 40 nm HP patterns performed with the $PSNA_{0.4}$ resist in different developers by EBL, which demonstrates the resolution limit and optimal exposure doses in different developers. It is difficult to obtain high resolution patterns in the pure *n*-BL developer. Only a 40 nm HP pattern with high roughness is given in the *n*-BL developer. Increasing the ratio of acetonitrile to *n*-BL in the developers from 1 : 2 to 2 : 1, and to pure acetonitrile, the resolutions and quality of the lithographic patterns are significantly improved, and a clear 25 nm HP pattern with no obvious defects is observed in acetonitrile, suggesting that acetonitrile is the optimal developer for the $PSNA_{0.4}$ resist.

Patterning properties of the $PSNA_{0.4}$ resist in EBL

The lithographic performance of the $PSNA_{0.4}$ resist for EBL was further investigated. The sensitivity and contrast of the $PSNA_{0.4}$ resist developed in acetonitrile were measured by the normalized remaining thickness (NRT) method with exposure to an e-beam of 100 keV. The exposure layout is shown in Fig. 1a with 36 frames (1 μm × 1 μm) in an array for exposure with an increasing dose on the resist film. The starting dose was set at 200 μC cm^{-2} and the dose increment was 8%. After exposure, the resist film was developed in acetonitrile for 60 s, and an extra 30 s rinsing in acetonitrile was conducted to remove the possible remains. The remaining thickness of the developed patterns was measured by AFM (Fig. 1b), giving the

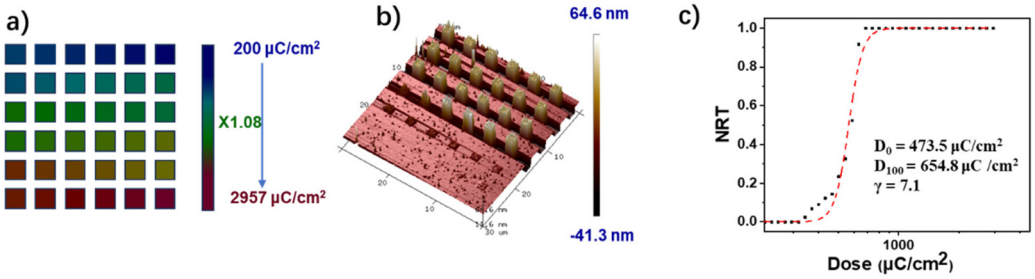

Fig. 1 The sensitivity and contrast analysis of the $PSNA_{0.4}$ resist for EBL: (a) layout file for normalized remaining thickness (NRT) testing, (b) three-dimensional AFM images of exposed $PSNA_{0.4}$ resist patterns at different doses, and (c) NRT curves for the $PSNA_{0.4}$ resist.

height of patterns with the increase in e-beam doses. Fig. 1c shows the contrast curve of the $PSNA_{0.4}$ resist, which can be further processed by fitting the NRT data using a logistic function. The sensitivity and contrast were calculated to be 654.8 μC cm^{-2} and 7.1 for the $PSNA_{0.4}$ resist according to our previously reported method.[49]

We also studied the impact of the resist thickness on the lithographic performance. Aspect ratio is a key factor for resist pattern formation since a high aspect ratio is preferred for pattern transfer using etching whereas a high aspect ratio may result in pattern collapse. Therefore, the patterning of $PSNA_{0.4}$ resist films with different thicknesses was studied by EBL. Fig. 2 shows the top-view SEM images of 25 nm L/S patterns for the $PSNA_{0.4}$ resist at film thicknesses of 44, 35, and 25 nm. In the case of 44 nm film thickness, the pattern collapse was clearly observed. Reducing the thickness to 35 nm, the collapse was completely suppressed and a clear pattern was obtained. Although the 25 nm L/S pattern can be achieved by reducing the film thickness to 25 nm, a substantial increase in line edge roughness (LER) is observed. This suggests that the poor soluble layer near the substrate leads to an increase in LER when the film thickness decreases. This is consistent with the previous report, which demonstrates that the low-energy secondary electrons are more likely to escape to the substrate in the case of a thinner resist film, resulting in a rise in reaction and poor solubility of the film near the substrate.[56] The aspect ratios for the patterns were estimated to be 1.8, 1.4, and 1.0 by dividing the film thickness (44, 35, and 25 nm) by the pattern width (25 nm). This suggests that the aspect ratio of 1.4 is accurate for the $PSNA_{0.4}$ resist resolving high resolution patterns in EBL, which is in agreement with our previous report.[29]

Fig. 3 shows SEM images of the 22 nm L/S patterns of the $PSNA_{0.4}$ resist at different exposure doses by EBL (thickness 30.0 nm). No obvious difference is observed for the line widths and LERs of the pattern in the dose range of 1400–1600 μC cm^{-2}. The $PSNA_{0.4}$ resist can form 23–24 nm HP patterns with LERs of 3.4–3.7 nm. Compared with previously reported molecular CARs,[57] the $PSNA_{0.4}$ resist as a n-CAR exhibits a larger exposure latitude. The LW and LER evolution at various exposure doses confirm the large exposure latitude for the $PSNA_{0.4}$ resist.

To demonstrate the resolution limit of the $PSNA_{0.4}$ resist, we further investigated the lithographic performance of smaller feature sizes under optimal conditions. Typical dense line patterns are shown in Fig. 4. The $PSNA_{0.4}$ resist can resolve 20 and 18 nm dense L/S patterns at a dose of 1300 μC cm^{-2} with LERs of 4.1 and 4.0 nm (Fig. S11 and S12†), respectively (Fig. 4a and b). A smaller dense L/S pattern of 16 nm suffers from blur and necking of lines (Fig. 4c), indicating the resolution limit of 18 nm for the $PSNA_{0.4}$ resist by EBL.

Patterning performance of the $PSNA_{0.4}$ resist for EUVL

The lithographic evaluation of the $PSNA_{0.4}$ resist was further carried out with EUV lithography tools. To ascertain the sensitivity and contrast of the $PSNA_{0.4}$ resist in EUV lithography, the

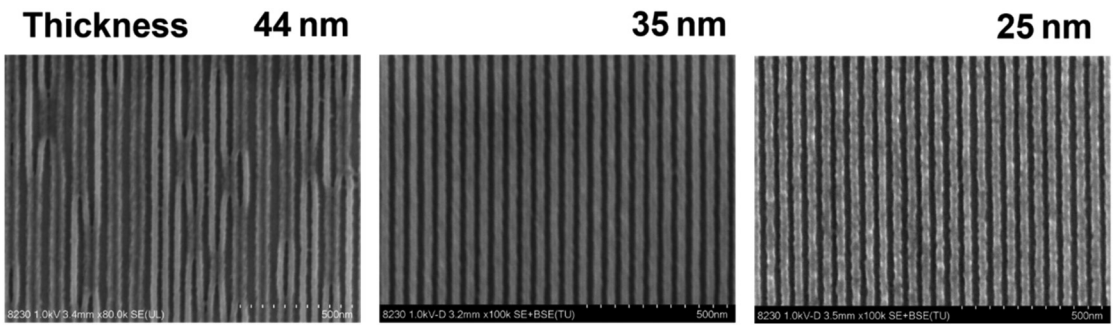

Fig. 2 SEM images of 25 nm L/S patterns (top view) for the $PSNA_{0.4}$ resist at different film thicknesses (exposure doses: 1600, 1415 and 1126 μC cm^{-2}).

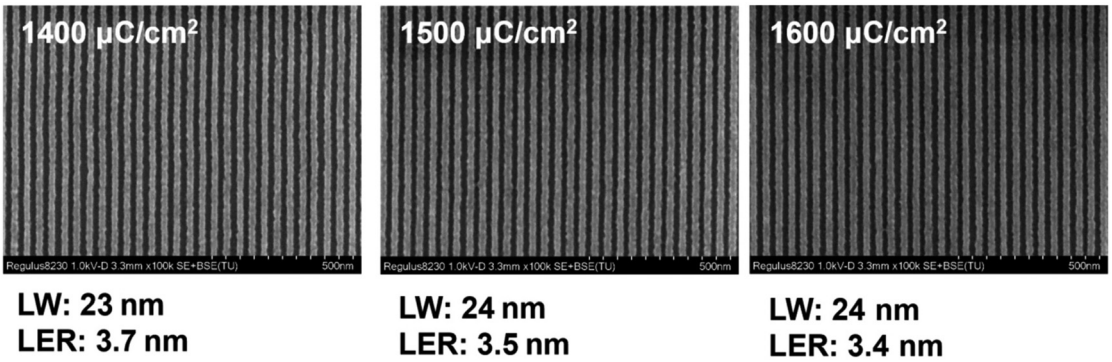

Fig. 3 SEM images of the patterns for the $PSNA_{0.4}$ resist at different exposure doses using 22 nm L/S layouts (film thickness: 30.0 nm).

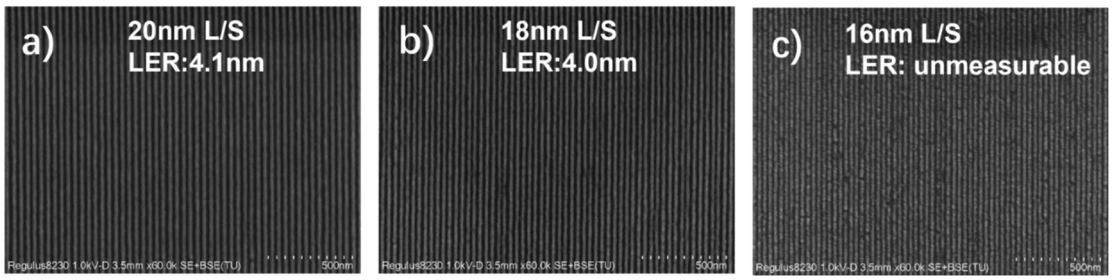

Fig. 4 High-resolution SEM images of the $PSNA_{0.4}$ resist for (a) 20 nm, (b) 18 nm, and (c) 16 nm L/S patterns by EBL at a dose of 1300 μC cm^{-2} (film thickness: 26 nm).

resist film with a thickness of 44 nm was exposed over a series of frames (0.5 × 0.5 mm^2) at different doses (increasing from 10 to 288 mJ cm^{-2}) of EUV radiation. After exposure, the resist film was developed in acetonitrile. The NRT plots were obtained by measuring the thickness variation of EUV exposed frames with doses in a similar way to that in EBL. By fitting the NRT curve with a logistic function, we were able to determine the D_0 and D_{100} to further calculate the contrast (γ) (Fig. S10†). The sensitivity and contrast of the $PSNA_{0.4}$ resist in EUV lithography were calculated to be 40.5 mJ cm^{-2} (D_{100}) and 5.2 (γ), respectively. It is worth noting that the sensitivity of the $PSNA_{0.4}$ resist was greatly improved compared with the sulfonium based n-CARs previously reported by our research group.[49,50] The reason for this will be discussed in the next section. To demonstrate the EUV lithography performance of the $PSNA_{0.4}$ resist, the feature sizes of 25 and 22 nm HP patterns were determined. Fig. 5 shows the SEM images of 25 and 22 nm HP patterns obtained by EUV lithography. The $PSNA_{0.4}$ resist can solve 25 and 22 nm HP patterns with high sensitivity rates of 97.2 and 90.8 mJ cm^{-2} and low LERs of 2.9 and 2.6 nm (Fig. S13 and S14†), respectively. It should be noted that the smaller feature size of HP patterns was not further

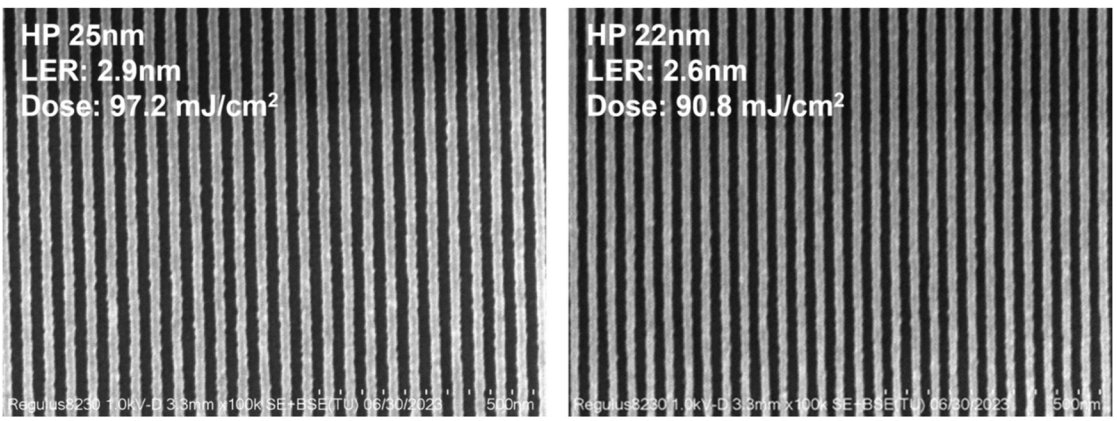

Fig. 5 SEM images of 25 and 22 nm HP patterns by EUV lithography.

optimized due to the upgrade of the Swiss Light Source (SLS). Although there is no higher resolution lithographic pattern by EUV lithography, we anticipate that the $PSNA_{0.4}$ resist has the potential to achieve higher resolution inferred from the results of EBL (18 nm L/S). Previous reports have confirmed that EUV lithography usually shows higher resolution than EBL because of the lower proximity effect of EUV patterning.[58,59]

Patterning mechanism of the $PSNA_{0.4}$ resist

EBL and EUVL are similar in generating secondary electrons to induce a photochemical reaction.[50] We analyzed the mechanism only by using the EBL method. To clarify the sensitive group change after e-beam exposure, an area (1.5 × 1.5 mm^2) of the $PSNA_{0.4}$ resist film was exposed to an e-beam at a dose of 3000 μC cm^{-2} and further developed in acetonitrile. An X-ray photoelectron spectroscopy (XPS) study was conducted to investigate the chemical bond changes of the material after e-beam exposure and development. Fig. S15–S17† show the high resolution XPS survey spectra of C 1s, O 1s, F 1s, S 2p, and I 3d envelopes for the $PSNA_{0.4}$ resist film before and after exposure, and after development, respectively. For the high resolution spectra of C 1s (Fig. 6a), the signals corresponding to the CF_3 (294.0 eV), CF_2 (291.7 eV), C═O (288.7 eV), C–I (285.5 eV), and C–C/C–H (284.8 eV) species for the pristine film can be identified according to the National Institute of Standards and Technology (NIST) XPS database and the pertinent literature.[60,61] After e-beam exposure and development, the signals of CF_3 and CF_2 gradually decreased to negligible, indicating the removal of the perfluoro-1-butanesulfonate anion. However, no obvious change of signals for C═O and C–I bonds was observed after exposure and development, which suggests that the naphthalimide group and the iodine containing product remain in the film residue after exposure and development. The XPS spectra of the I 3d envelop are shown in Fig. 6b. The peak split corresponds to the orbital split of I 3d to $3d_{3/2}$ and $3d_{5/2}$ levels. Therefore, the I 3d spectrum of the $PSNA_{0.4}$ pristine resist film can be divided into two couples of peaks [620.6 eV ($3d_{5/2}$) and 631.6 eV ($3d_{3/2}$), and 622.1 eV ($3d_{5/2}$) and 633.5 eV ($3d_{3/2}$)]. The binding energies of 620.6 eV and 631.6 eV are in agreement with the binding energies of Ar–I,[62] while the binding energies of 622.1 eV and 633.5 eV are ascribed to the iodonium species.[63] This suggests that the iodonium structure in the $PSNA_{0.4}$ resist film is partly hydrolyzed due to moisture, according to the literature.[63] After exposure to the electron beam, the vanishing peaks at 622.1 eV and 633.5 eV indicate the decomposition of the iodonium structure. The resulting Ar–I product remains in the film after development. Similar structures of molecular iodonium salts have been reported by Lalevée *et al.*[55,64] They demonstrate that the bond dissociation energy (BDE) of the C–I bonds that compose iodonium can be measured by molecular orbital calculations, supporting that the cleavage of the C–I bond linked to PS is more favored due to the lower BDE. Based on the above knowledge, we propose a mechanism of how $PSNA_{0.4}$ decomposes under e-beam irradiation and forms the solubility switch after development, as shown in Fig. 6c. During e-beam irradiation, the bond cleavage occurs mainly at the PS–I^+ bond for the biphenyl iodonium group, resulting in the radical species $PS^{\bullet}$ and Naph-Ar-$I^{+\bullet}$. The following cross-linking of $PS^{\bullet}$ coupling with Naph-Ar-$I^{+\bullet}$ to release H^+ results in the switch of the solubility of the film in acetonitrile.

The sensitivity (D_{100} = 40.5 mJ cm^{-2}) of the $PSNA_{0.4}$ resist is greatly improved compared with the sulfonium based polymeric PSTS n-CARs (D_{100} = 141 mJ cm^{-2}) reported by our research group.[49] To clarify the reason for the increased sensitivity, we calculated the bond energy of the C–I bond that

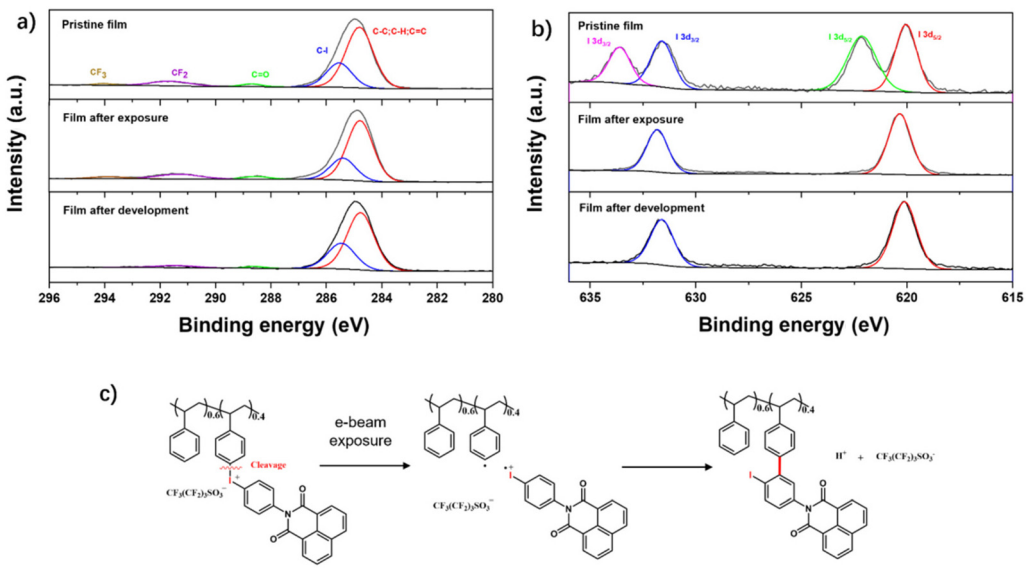

Fig. 6 The XPS analysis of the $PSNA_{0.4}$ resist film. (a) C 1s, (b) I 3d envelope of the $PSNA_{0.4}$ resist films before and after e-beam irradiation, and after development. (c) The proposed decomposition pathway of $PSNA_{0.4}$ by e-beam irradiation.

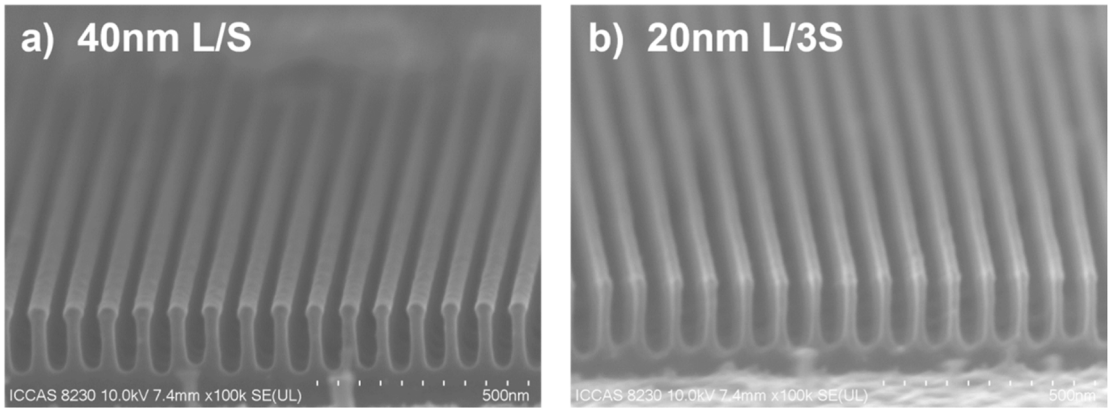

Fig. 7 Cross-section profiles of the transferred (a) 40 nm L/S and (b) 20 nm L/3S patterns on a Si substrate.

formed iodonium in $PSNA_{0.4}$ and the C–S bond of sulfonium in PSTS by M062X/Def2TZVP of Gaussian 09 optimized with wB97XD/Def2SVP.[65] It is demonstrated that the bond energy of the C–I bond in $PSNA_{0.4}$ was 359.6 kJ mol^{-1}, while the smallest bond energy of the C–S bond in sulfonium was 502.9 kJ mol^{-1}. This suggests that the iodonium group in $PSNA_{0.4}$ is more feasible to be cleaved by EUV irradiation than the sulfonium group in PSTS. Moreover, the EUV absorption cross-section of the iodine atom is much higher than that of the sulfur atom,[66] which increases the absorption of the film for EUV photons and thus improves the yield of secondary electrons that induce the photochemical reactions. In summary, the low bond energy of the C–I bond in iodonium and the large EUV absorption cross-section of the iodine atom contribute to the high sensitivity of the $PSNA_{0.4}$ resist.

Etch resistance and pattern transfer capability of the $PSNA_{0.4}$ resist

The etching resistance is an important parameter when transferring resist patterns on the Si substrate. The etching rate of the $PSNA_{0.4}$ resist films after development was evaluated by using an SF_6/O_2 mixture plasma. After etching, resist stripping was performed in THF and DMSO in an ultrasonic bath for 5 min, respectively. Fig. S18† shows the three-dimensional (3D) AFM topography image of the $PSNA_{0.4}$ resist pattern after development (Fig. S18a†), etching for 10 s (Fig. S18b†) and resist stripping (Fig. S18c†), where the etching depth is calculated by using the height difference. The $PSNA_{0.4}$ resist film was 34.0 nm before etching, according to Fig. S18a.† Then the remaining thickness of the $PSNA_{0.4}$ resist film after etching was calculated to be 13 nm from the thickness difference before and after etching. Therefore, the etching depths of the $PSNA_{0.4}$ resist film and Si substrate were 21 and 200 nm, giving etching rates of 2.1 and 20.0 nm s^{-1}, respectively. The etching selectivity of the $PSNA_{0.4}$ resist to the Si substrate was calculated to be 9.5 : 1. The pattern transfer capability of the $PSNA_{0.4}$ resist was evaluated under the same etching conditions. Fig. 7a and b show the cross-sectional profiles of the transferred patterns of 40 nm L/S and 20 nm L/3S patterns after etching on silicon. The critical dimensions of the transferred patterns are consistent with the original resist patterns (Fig. S19a and 19b†). The aspect ratios of the patterns are approximately 5 : 1, maintaining original line widths of 40 and 20 nm. This demonstrates the excellent ability of the $PSNA_{0.4}$ resist in high resolution pattern transferring, suggesting its potential application in the IC industry.

Conclusions

In summary, we prepared an iodonium modified polystyrene ($PSNA_{0.4}$) based non-chemically amplified resist. The $PSNA_{0.4}$ resist can resolve dense line patterns of 18 nm L/S at a dose of 1300 μC cm^{-2} *via* negative tone development. Further EUV lithographic performance demonstrates that the $PSNA_{0.4}$ resist can achieve 22 nm L/S patterns at a dose of 90.8 mJ cm^{-2}. Our previous reports demonstrated that the EUV exposure doses for triphenylsulfonium based resists are ~200 mJ cm^{-2} at the same resolution. The sensitivity of the $PSNA_{0.4}$ resist is significantly improved compared with sulfonium-functionalized resists, which is attributed to the high absorption cross-section for EUV photons and the lower bond energy of the C–I bond in iodonium compared with that of the C–S bond in the sulfonium group. The studies on the underlying exposure mechanism suggest the decomposition of polar iodonium into nonpolar PS or iodobenzene species, resulting in the solubility switch of the $PSNA_{0.4}$ resist film. This work demonstrates that the integration of iodonium into polymers provides a novel pathway in the endeavor of enhancing the EUV sensitivity of n-CARs.

Experimental sections

Chemicals and reagents

All the standard reagents and chemicals were purchased from commercial sources and used without any further purification.

Instrument

NMR spectra were recorded on an Avance II-600 spectrometer (Bruker, Germany). The molecular weight (M_w) and the polydispersity index (PDI) of PS used to synthesize $PSNA_{0.4}$ were determined by performing gel permeation chromatography analyses (GPC, Wyatt DAWN Series). THF was used as the mobile phase at a flow rate of 1.0 mL min^{-1}. Fourier transform infrared (FT-IR) spectra were recorded using an Excalibur 3100 IR spectrometer (Varian, USA). Thermogravimetric analysis and DSC were performed on TGA 4000 (PerkinElmer, USA) and DSC 4000 (PerkinElmer, USA) instruments at a heating rate of 10 °C min^{-1}, respectively. The thin films were prepared with a coating machine (Brewer Science CEE/200X, USA). The resist film thickness was measured using a spectroscopic ellipsometer (Angstrom Sun/AST SE200BM, USA). AFM (Bruker/Dimension FastscanBio system, USA) was employed to determine the surface morphology of $PSNA_{0.4}$ resist films. UV (254 nm) exposure experiments were performed on a CEL-LPH120-254 (Beijing China Education Au-light Co., Ltd). E-beam exposure experiments were performed on a Vistec EBPG 5000plus ES (Vistec, USA). The acceleration voltage and beam current were 100 kV and 100 pA, respectively. SEM (Regulus 8230, Japan) equipment was used to characterize the top-view patterns. The LER was measured by analyzing SEM images with ProSEM software. The exposure films were characterized using X-ray photoelectron spectroscopy (Thermo Scientific/ESCALAB 250Xi, UK). The etching step was performed on a plasma etching machine (Sentech/Etchlab 200, Germany) after the patterning process.

Procedure for the synthesis of polystyrene

Polystyrene was prepared according to the previous report of our group.[48] The synthesized polystyrene was evaluated using ^{1}H NMR and GPC (Fig. S1 and S2†).

Procedure for the synthesis of *N*-(*p*-iodophenyl)-1,8-naphthalimide

N-(*p*-Iodophenyl)-1,8-naphthalimide was prepared according to the literature.[55] The synthesized *N*-(*p*-iodophenyl)-1,8-naphthalimide was evaluated using ^{1}H NMR (Fig. S3†).

Procedure for the synthesis of $PSNA_{0.4}$

PS (470 mg, 0.1 mmol, M_w = 4700) and *N*-(*p*-iodophenyl)-1,8-naphthalimide (520 mg, 1.3 mmol) were dissolved in dichloromethane (15 mL) at 0 °C and then 3-chloroperoxybenzoic acid (85%) (340 mg, 17 mmol) was added to the reaction mixture. After stirring for 10 min, 1-perfluoro-1-butanesulfonic acid (510 mg, 17 mmol) was dropped in and the reaction continued at 0 °C for about 1 h. The ice bath was removed and the reaction continued at room temperature for about 24 h. After the reaction, the reaction solution was poured into diethyl ether and precipitation was repeated three times with diethyl ether. The precipitates were filtered and vacuum-dried at 50 °C to obtain yellowish products (900 mg). FTIR: ν_{max}/cm^{-1} 1673 (C═O), 3026 and 2926 (CH), 1269 (CF_3), 1133 and 659 (SO_2), 1054 (S–O), 527 (C–I). ^{1}H NMR (400 MHz, acetonitrile-d_3) δ (ppm) 8.50 (s, 0.5H), 8.39 (s, 0.5H), 8.13 (s, 1H), 7.81 (s, 1H), 7.55 (s, 1H), 7.10 (s, 3H), 6.59 (s, 2H), 1.2–1.8 (s, 3H).

General procedure for $PSNA_{0.4}$ resist lithography

The $PSNA_{0.4}$ material was dissolved in acetonitrile, making a 15 mg mL^{-1} solution. The solution was filtered through a 0.2 μm membrane filter 3 times and spin-coated on silicon wafers to form thin films. A post-application bake at 90 °C for 120 s was applied to resist the films using a hot plate to remove excess casting solvent. The film thickness was measured using a spectroscopic ellipsometer, and the film was then exposed to e-beam or EUV irradiation. The EUV patterning properties of resists were studied by using the EUV interference lithography tool at the XIL-II beamline in the Swiss Light Source. After exposure, the wafers were immersed in acetonitrile for 60 s and then rinsed with the same solvent for 30 s before drying. The resulting patterns were inspected using SEM or AFM. The LER parameters for all the patterns were analyzed using ProSEM software. All the lines in the image were selected for analysis, and the LERs on the left and the right were obtained. Their average value was taken as the LER value of the image.

Contrast and sensitivity analysis

A series of square exposure patterns (1 μm) with different exposure doses were made by electron beam exposure. After development, contrast curves were obtained by measuring the remaining film thickness of the square area using AFM.

Exposure mechanism investigation

To analyze compositional changes after e-beam exposure, the $PSNA_{0.4}$ resist films were exposed over a large area of 1.5 × 1.5 mm^2 with an electron energy of 100 kV, a current of 100 nA, and a dose of 3000 μC cm^{-2}. The unexposed, exposed, and developed wafers were characterized by XPS.

Etching conditions

The plasma conditions were set at a 30 sccm SF_6 and a 15 sccm O_2 gas flow, a RF power of 5 W, and an ICP power of 300 W. The pressure in the process chamber was 7 mTorr and the table temperature was −110 °C.

Data availability

The data supporting this article have been included as part of the ESI.†

Author contributions

X. Y. performed the synthesis, experimental measurements, and manuscript drafting. P. L. was involved in the theoretical calculation of bond energy. J. C. proposed the idea, conducted the experiments, analyzed the data, and performed the manu-

script review. Y. Z., T. Y., S. W., X. G., and R. H. were involved in the design of experiments, analytical characterization, data analysis, and discussions. P. T., M. V., and D. K. performed the EUV lithographic experiment. Y. E. was involved in the design of EUV experiments and manuscript review. G. Y. helped with the data analysis, discussions, and manuscript review. Y. L. supervised the overall study and the manuscript review.

Conflicts of interest

The authors declare no competing financial interest.

Acknowledgements

This work was supported by the National Natural Science Foundation of China (22090012 and U20A20144). Support (YZQT020) from the Chinese Academy of Sciences (CAS) is gratefully acknowledged. We are also thankful to the National Center for Nanoscience and Technology for EBL and etching experiments. Parts of this work were performed at the Swiss Light Source, SLS, Paul Scherrer Institute.

References

1 G. E. Moore, *Proceedings of SPIE*, *Optical/Laser Microlithography VIII Conference*, 1995, vol. 2440, pp. 2–17.
2 L. Li, X. Liu, S. Pal, S. Wang, C. K. Ober and E. P. Giannelis, *Chem. Soc. Rev.*, 2017, **46**, 4855–4866.
3 E. Reichmanis, F. M. Houlihan, O. Nalamasu and T. X. Neenan, *Chem. Mater.*, 1991, **3**, 394–407.
4 S. Hu, J. Chen, T. Yu, Y. Zeng, X. Guo, S. Wang, G. Yang and Y. Li, *J. Photochem. Photobiol., A*, 2023, **436**, 114351.
5 J. Chen, Q. Hao, S. Wang, S. Li, T. Yu, Y. Zeng, J. Zhao, S. Yang, Y. Wu, C. Xue, G. Yang and Y. Li, *ACS Appl. Polym. Mater.*, 2019, **1**, 526–534.
6 J. Jiang, D. De Simone, O. Yildirim, M. Meeuwissen, R. Hoefnagels, G. Rispens, R. Custers and P. Derks, *Proceedings of SPIE*, *Conference on Extreme Ultraviolet (EUV) Lithography VIII*, 2017, vol. 10143, p. 1014323.
7 T. Kozawa, *Jpn. J. Appl. Phys.*, 2012, **51**, 116503.
8 Y. Wang, J. Yuan, J. Chen, Y. Zeng, T. Yu, X. Guo, S. Wang, G. Yang and Y. Li, *ACS Omega*, 2023, **8**, 12173–12182.
9 W. T. James, *J. Micro/Nanolithogr., MEMS, MOEMS*, 2011, **10**, 1–9.
10 D. N. Tuan, H. Yamamoto and S. Tagawa, *Jpn. J. Appl. Phys.*, 2012, **51**, 086503.
11 J. H. Jung, M. J. Kim, K. H. Sohn, H. N. Kang, M. K. Kang and H. Lee, *J. Nanosci. Nanotechnol.*, 2015, **15**, 1764–1766.
12 T. Kozawa, J. J. Santillan and T. Itani, *Appl. Phys. Express*, 2012, **5**, 074301.
13 T. Kozawa, *Jpn. J. Appl. Phys.*, 2015, **54**, 126501.
14 C. Popescu, Y. Vesters, A. McClelland, D. De Simone, G. Dawson, J. Roth, W. Theis, G. Vandenberghe and A. P. G. Robinson, *J. Photopolym. Sci. Technol.*, 2018, **31**, 227–232.
15 J. Gao, S. Zhang, X. Cui, X. Cong, X. Guo, R. Hu, S. Wang, J. Chen, Y. Li and G. Yang, *Adv. Mater. Interfaces*, 2023, **10**, 2300194.
16 S. Zhang, L. Chen, J. Gao, X. Cui, X. Cong, X. Guo, R. Hu, S. Wang, J. Chen, Y. Li and G. Yang, *ACS Omega*, 2023, **8**, 26739–26748.
17 V. Singh, V. S. V. Satyanarayana, S. K. Sharma, S. Ghosh and K. E. Gonsalves, *J. Mater. Chem. C*, 2014, **2**, 2118–2122.
18 B. Cardineau, P. Garczynski, W. Earley and R. L. Brainard, *J. Photopolym. Sci. Technol.*, 2013, **26**, 665–671.
19 A. Shirotori, Y. Vesters, M. Hoshino, A. Rathore, D. De Simone, G. Vandenberghe and H. Matsumoto, *Proceedings of SPIE*, *International Conference on Extreme Ultraviolet Lithography (EUVL)*, 2019, vol. 11147, p. 111470J.
20 J. Deng, S. Bailey, S. Jiang and C. K. Ober, *J. Am. Chem. Soc.*, 2022, **144**, 19508–19520.
21 J. Deng, S. Bailey, R. Ai, A. Delmonico, G. Denbeaux, S. Jiang and C. K. Ober, *ACS Macro Lett.*, 2022, 1049–1054, DOI: **10.1021/acsmacrolett.2c00395**.
22 H. H. Solak, Y. Ekinci, P. Käser and S. Park, *J. Vac. Sci. Technol., B: Microelectron. Nanometer Struct.–Process., Meas., Phenom.*, 2007, **25**, 91–95.
23 K. J. Lawrie, I. Blakey, J. P. Blinco, H. H. Cheng, R. Gronheid, K. S. Jack, I. Pollentier, M. J. Leeson, T. R. Younkin and A. K. Whittaker, *J. Mater. Chem.*, 2011, **21**, 5629–5637.
24 A. G. Yu, H. P. Liu, J. P. Blinco, K. S. Jack, M. Leeson, T. R. Younkin, A. K. Whittaker and I. Blakey, *Macromol. Rapid Commun.*, 2010, **31**, 1449–1455.
25 X.-Y. Lu, H. Luo, K. Wang, Y.-Y. Zhang, X.-F. Zhu, D. Li, B. Ma, S. Xiong, P. F. Nealey, Q. Li and G.-P. Wu, *Adv. Funct. Mater.*, 2021, **31**, 2007417.
26 A. Frommhold, D. X. Yang, A. McClelland, X. Xue, R. E. Palmer and A. P. G. Robinson, *Proc. SPIE*, 2013, **8682**, 86820Q.
27 F. Tatsuya, M. Shogo, Y. Tomotaka, K. Yoshitaka, K. Daisuke and O. Katsumi, *Proc. SPIE*, 2016, **9776**, 97760Y.
28 Y. Wang, J. Chen, Y. Zeng, T. Yu, X. Guo, S. Wang, T. Allenet, M. Vockenhuber, Y. Ekinci, J. Zhao, S. Yang, Y. Wu, G. Yang and Y. Li, *ACS Omega*, 2022, **7**, 29266–29273.
29 S. Hu, J. Chen, T. Yu, Y. Zeng, S. Wang, X. Guo, G. Yang and Y. Li, *J. Mater. Chem. C*, 2022, **10**, 9858–9866.
30 B. Cardineau, R. Del Re, H. Al-Mashat, M. Marnell, M. Vockenhuber, Y. Ekinci, C. Sarma, M. Neisser, D. A. Freedman and R. L. Brainard, Proceedings of SPIE, Conference on Advances in Patterning Materials and Processes XXXI, 2014, vol. 9051, p. 90511B.
31 S. Kataoka and K. Sue, *Eur. J. Inorg. Chem.*, 2022, **2022**, e202200050.
32 N. Thakur, R. Bliem, I. Mochi, M. Vockenhuber, Y. Ekinci and S. Castellanos, *J. Mater. Chem. C*, 2020, **8**, 14499–14506.

33 S. K. Sharma, R. Kumar, M. Chauhan, M. G. Moinuddin, J. Peter, S. Ghosh, C. P. Pradeep and K. E. Gonsalves, *Proceedings of SPIE*, *Conference on Advances in Patterning Materials and Processes XXXVII*, 2020, vol. 11326, p. 1132604.
34 S. Chakrabarty, C. Ouyang, M. Krysak, M. Trikeriotis, K. Cho, E. P. Giannelis and C. K. Ober, Proceedings of SPIE, Conference on Extreme Ultraviolet (EUV) Lithography IV, 2013, vol. 8679, p. 867906.
35 C. Y. Ouyang, Y. S. Chung, L. Li, M. Neisser, K. Cho, E. P. Giannelis and C. K. Ober, Proceedings of SPIE, Conference on Advances in Resist Materials and Processing Technology XXX, 2013, vol. 8682, p. 86820R.
36 M. Siauw, K. Du, D. Valade, P. Trefonas, J. W. Thackeray, A. Whittaker and I. Blakey, Proceedings of SPIE, Conference on Advances in Patterning Materials and Processes XXXIII, 2016, vol. 9779, p. 97790J.
37 X. Hong, Y. Kou, S. Kazunori, K. Vasiliki, K. Kazuki, P. G. Emmanuel and K. O. Christopher, *Proc. SPIE*, 2018, **10583**, 105831P.
38 J. Passarelli, M. Murphy, R. Del Re, M. Sortland, L. Dousharm, M. Vockenhuber, Y. Ekinci, M. Neisser, D. A. Freedman and R. L. Brainard, Proceedings of SPIE, Conference on Advances in Patterning Materials and Processes XXXII, 2015, vol. 9425, p. 94250T.
39 J. Passarelli, M. Sortland, R. Del Re, B. Cardineau, C. Sarma, D. A. Freedman and R. L. Brainard, *J. Photopolym. Sci. Technol.*, 2014, **27**, 655–661.
40 J. Sitterly, M. Murphy, S. Grzeskowiak, G. Denbeaux and R. L. Brainard, Proceedings of SPIE, Conference on Advances in Patterning Materials and Processes XXXV, 2018, vol. 10586, p. 105861P.
41 G. K. Belmonte, S. W. Cendrond, P. G. Reddy, C. A. S. Moura, M. G. Moinuddin, J. Peter, S. K. Sharma, G. A. Lando, M. Puiatti, K. E. Gonsalves and D. E. Weibel, *Appl. Surf. Sci.*, 2020, **533**, 146553.
42 Y. Si, Y. Zhao, G. Shi, D. Zhou, F. Luo, P. Chen, J. Fan and X. Peng, *J. Mater. Chem. A*, 2023, **11**, 4801–4807.
43 P. G. Reddy, S. P. Pal, P. Kumar, C. P. Pradeep, S. Ghosh, S. K. Sharma and K. E. Gonsalves, *ACS Appl. Mater. Interfaces*, 2017, **9**, 17–21.
44 V. S. V. Satyanarayana, V. Singh, V. Kalyani, C. P. Pradeep, S. Sharma, S. Ghosh and K. E. Gonsalves, *RSC Adv.*, 2014, **4**, 59817–59820.
45 P. G. Reddy, P. Kumar, S. Ghosh, C. P. Pradeep, S. K. Sharma and K. E. Gonsalves, *Mater. Chem. Front.*, 2017, **1**, 2613–2619.
46 J. Peter, M. G. Moinuddin, S. Ghosh, S. K. Sharma and K. E. Gonsalves, *ACS Appl. Polym. Mater.*, 2020, **2**, 1790–1799.
47 M. Yogesh, M. G. Moinuddin, M. Chauhan, S. K. Sharma, S. Ghosh and K. E. Gonsalves, *ACS Appl. Electron. Mater.*, 2021, **3**, 1996–2004.
48 Z. Wang, J. Chen, T. Yu, Y. Zeng, G. Yang, T. Allenet, V. Michaela, E. Yasin and Y. Li, *J. Micro/Nanopatterning, Mater., Metrol.*, 2022, **21**, 041403.
49 Z. Wang, J. Chen, T. Yu, Y. Zeng, X. Guo, S. Wang, T. Allenet, M. Vockenhuber, Y. Ekinci, G. Yang and Y. Li, *ACS Appl. Mater. Interfaces*, 2023, **15**, 2289–2300.
50 Y. Wang, J. Chen, Y. Zeng, T. Yu, S. Wang, X. Guo, R. Hu, P. Tian, M. Vockenhuber, D. Kazazis, Y. Ekinci, Y. Wu, S. Yang, J. Zhao, G. Yang and Y. Li, *ACS Appl. Nano Mater.*, 2023, **6**, 18480–18490.
51 C. D. Higgins, C. R. Szmanda, A. Antohe, G. Denbeaux, J. Georger and R. L. Brainard, *Jpn. J. Appl. Phys.*, 2011, **50**, 036504.
52 C. Higgins, A. Antohe, G. Denbeaux, S. Kruger, J. Georger and R. Brainard, *Proceedings of SPIE*, *Conference on Alternative Lithographic Technologies*, 2009, vol. 7271, p. 727147.
53 D. L. Goldfarb, A. Afzali-Ardakani and M. Glodde, Proceedings of SPIE, Conference on Advances in Patterning Materials and Processes XXXIII, 2016, vol. 9779, p. 97790A.
54 J. V. Crivello and E. Reichmanis, *Chem. Mater.*, 2013, **26**, 533–548.
55 S. Villotte, D. Gigmes, F. Dumur and J. Lalevée, *Molecules*, 2020, **25**, 149.
56 N. Maeda, A. Konda, K. Okamoto, T. Kozawa and T. Tamura, *Jpn. J. Appl. Phys.*, 2020, **59**, 086501.
57 S. Hu, J. Chen, T. Yu, Y. Zeng, G. Yang and Y. Li, *Chem. Res. Chin. Univ.*, 2022, **39**, 139–143.
58 B. Suchit, C. Weilun, R. N. Andrew and P. N. Patrick, *Proc. SPIE*, 2014, **9048**, 90481H.
59 S. Bhattarai, A. R. Neureuther and P. P. Naulleau, *J. Vac. Sci. Technol., B: Nanotechnol. Microelectron.: Mater., Process., Meas., Phenom.*, 2017, **35**, 061602.
60 G. K. Belmonte, C. A. S. Moura, P. G. Reddy, K. E. Gonsalves and D. E. Weibel, *J. Photochem. Photobiol., A*, 2018, **364**, 373–381.
61 A. Chilkoti and B. D. Ratner, *Chem. Mater.*, 1993, **5**, 786–792.
62 H. F. Wang, X. Y. Deng, J. Wang, X. F. Gao, G. M. Xing, Z. J. Shi, Z. N. Gu, Y. F. Liu and Y. L. Zhao, *Acta Phys.-Chim. Sin.*, 2004, **20**, 673–675.
63 A. Hartwig, A. Harder, A. Lühring and H. Schröder, *Eur. Polym. J.*, 2001, **37**, 1449–1455.
64 N. Zivic, M. Bouzrati-Zerrelli, S. Villotte, F. Morlet-Savary, C. Dietlin, F. Dumur, D. Gigmes, J. P. Fouassier and J. Lalevée, *Polym. Chem.*, 2016, **7**, 5873–5879.
65 V. K. Prasad, Z. P. Pei, S. Edelmann, A. Otero-de-la-Roza and G. A. DiLabio, *J. Chem. Theory Comput.*, 2022, **18**, 151–166.
66 R. Fallica, J. Haitjema, L. Wu, S. C. Ortega, A. M. Brouwer and Y. Ekinci, *J. Micro/Nanolithogr., MEMS, MOEMS*, 2018, **17**, 023505.